

Lieb-Liniger-like model of quantum solvation in CO- $^4\text{He}_N$ clusters

D. Farrelly,^{1,2,a)} M. Iñarrea,³ V. Lanchares,² and J. P. Salas³

¹Departamento de Matemáticas y Computación, Universidad de La Rioja, 26006 Logroño, Spain

²Department of Chemistry and Biochemistry, Utah State University, Logan, Utah 84322-0300, USA

³Área de Física Aplicada, Universidad de La Rioja, 26006 Logroño, Spain

(Received 17 March 2016; accepted 2 May 2016; published online 23 May 2016)

Small ^4He clusters doped with various molecules allow for the study of “quantum solvation” as a function of cluster size. A peculiarity of quantum solvation is that, as the number of ^4He atoms is increased from $N = 1$, the solvent appears to decouple from the molecule which, in turn, appears to undergo free rotation. This is generally taken to signify the onset of “microscopic superfluidity.” Currently, little is known about the quantum mechanics of the decoupling mechanism, mainly because the system is a quantum $(N + 1)$ -body problem in three dimensions which makes computations difficult. Here, a one-dimensional model is studied in which the ^4He atoms are confined to revolve on a ring and encircle a rotating CO molecule. The Lanczos algorithm is used to investigate the eigenvalue spectrum as the number of ^4He atoms is varied. Substantial solvent decoupling is observed for as few as $N = 5$ ^4He atoms. Examination of the Hamiltonian matrix, which has an almost block diagonal structure, reveals increasingly weak inter-block (solvent-molecule) coupling as the number of ^4He atoms is increased. In the absence of a dopant molecule the system is similar to a Lieb-Liniger (LL) gas and we find a relatively rapid transition to the LL limit as N is increased. In essence, the molecule initially—for very small N —provides a central, if relatively weak, attraction to organize the cluster; as more ^4He atoms are added, the repulsive interactions between the identical bosons start to dominate as the solvation ring (shell) becomes more crowded which causes the molecule to start to decouple. For low N , the molecule pins the atoms in place relative to itself; as N increases the atom-atom repulsion starts to dominate the Hamiltonian and the molecule decouples. We conclude that, while the notion of superfluidity is a useful and correct *description* of the decoupling process, a molecular viewpoint provides complementary insights into the quantum mechanism of the transition from a molecular cluster to a quantum solvated molecule. *Published by AIP Publishing.* [<http://dx.doi.org/10.1063/1.4949537>]

I. INTRODUCTION

Superfluidity is often thought of as being an essentially macroscopic phenomenon with ^4He ^{1,2} and ^3He ³ being the most common, or at least the most conveniently accessible,^{4,5} examples—although superfluidity has recently been observed in ultra-cold atomic gases.⁶ However, early path integral Monte Carlo (PIMC) calculations predicted that microscopic droplets of ^4He , containing as few as 64 atoms, would be superfluid at low enough temperature.⁷ The earliest *experimental* evidence that small ^4He droplets might be superfluid came from studies of ^4He nanodroplets doped with glyoxal molecules⁸ together with later studies which investigated the spectra of OCS and SF₆ dopants^{9,10}—see also Refs. 11 and 12. Remarkably, these spectra indicated apparent free rotation of the OCS and SF₆ molecules inside the droplet. Free rotation was suggested by very sharp rotational lines, reminiscent of a gas phase spectrum, although with altered rotational constants; that is, the apparent moment of inertia of the dopant was larger than its gas phase value but smaller than expected classically. Since then a large number of molecules

have been observed to display similar behavior.^{13–16} The most logical—and the original—explanation was that molecules undergo almost-frictionless rotation in a microscopic analog of the Andronikashvili experiment.¹⁰ The behavior of the moment of inertia was attributed, in a later theoretical study,¹⁷ to a portion of the ^4He density “adiabatically following” the rotation of the molecule, an idea that was later tested experimentally.¹⁸

Grebenev *et al.*¹⁰ originally proposed that 60 ^4He atoms were necessary for superfluidity but later work found that microscopic superfluidity can arise in even smaller clusters, containing only 9 solvent atoms.²³ Pure microwave spectra collected for a variety of similarly small doped bosonic clusters, composed of ^4He atoms or $p\text{-H}_2$ molecules, have since been obtained,^{26–32} and rather remarkably, indicate that atomic scale superfluidity may, in fact, occur for as few as 3–5 bosons. The evidence is as follows: the effective moments of inertia of a variety of impurity molecules in $^4\text{He}_N$ (or $p\text{-(H}_2)_N$) clusters appear initially to increase with N , as expected classically. However, a turning point is reached when the moment of inertia commences a nonclassical decrease with the molecule eventually undergoing almost free rotation inside the cluster. However, the asymptotic (in N) value of the moment of inertia—the nanodroplet limit—is larger than for the free

^{a)}Permanent address: Department of Chemistry and Biochemistry, Utah State University, Logan, Utah 84322-0300, USA.

molecule. The precise value of N at which the observed moment of inertia starts to decrease depends sensitively on the molecule. The downturn in the moment of inertia can also be thought of as an upturn in the effective rotational constant of the molecule (B_{eff}). This behavior is an indication that the molecule has started to decouple from the bosonic “solvent” and it is this turnaround which is taken to signal the onset of microscopic superfluidity.^{22–25}

Recent experiments have directly confirmed superfluidity in ^4He droplets by observing a critical Landau velocity in droplets containing $\sim 10^6$ atoms¹⁹ and by imaging quantized vortices in droplets containing $\sim 10^8$ – 10^{11} atoms.²⁰ However, while the term “superfluidity” provides a compelling description of experimental observations, a molecular picture provides complementary insights into the transition from a small molecular complex to a quantum solvated dopant. The picture is somewhat clouded by the fact that, in the literature, superfluidity does not always have a unique definition, especially in microscopic or reduced dimensionality situations; for example, according to Ref. 21, superfluidity is best thought of as a “complex cluster of phenomena.” It is, therefore, important to emphasize that the term “microscopic (or atomic scale) superfluidity,” as often used in the context of doped helium droplets in the chemical physics literature, does not necessarily imply a microscopic system that displays the complete range of properties generally associated with He^{II} .²⁶ Rather, the term most often refers, specifically, to the nonclassical turnaround of the moment of inertia as a function of cluster size. It is possible that different aspects of superfluidity (frictionless flow, quantized vortices, nonclassical behavior of the moment of inertia, etc.²¹) will appear at different sized cluster sizes.

Naturally, these observations and considerations have precipitated computational studies into the connection between microscopic and macroscopic superfluidity^{24,25} for example, using PIMC calculations. The PIMC method utilizes an isomorphism between the actual quantum problem and a classical system of “bead and spring” ring polymers.⁷ Superfluidity manifests itself when the polymers “cross-link” and an “area estimator” can be used to compute the fractions of normal and superfluid components.⁷ Using this method recent finite temperature simulations have identified normal and superfluid components in CO_2 - $^4\text{He}_N$ and CO -(p - H_2) $_N$ clusters.^{31,33} The calculations for CO -(p - H_2) $_N$ clusters yield two remarkable results:³¹ (i) a superfluid component is calculated for $N = 1$ while (ii) for $N > 10$ the CO molecule undergoes completely free rotation with no apparent reduction in its rotational constant. In contrast, for CO - $^4\text{He}_N$ clusters with $N \sim 10$ the effective rotational constant is observed experimentally to lie close to the converged nanodroplet limit which is somewhat lower than the gas-phase value.^{30,31,34} Clearly, these simulations add validity to the notion that superfluidity is in some way behind the observed turnaround in the effective rotational constant. However, while PIMC calculations are a computational diagnostic of the presence of a superfluid component, having to view the results through the prism of a classical isomorphism provides a less direct route to understanding the actual quantum mechanism than does a variational calculation. Similarly, diffusion Monte Carlo

(DMC) calculations can reproduce accurately the observed turnaround in the effective rotational constant for a variety of molecules, but yield less insight into the details how and why this behavior occurs. Unfortunately, the many-body nature of doped ^4He clusters makes them difficult to study computationally except using quantum Monte Carlo methods.

To avoid some of the aforementioned difficulties, in previous work, a simplified model of the intensively studied CO - $^4\text{He}_N$ -complex was introduced in which the ^4He atoms were confined to a ring—the bosons on a ring (BOAR) model³⁵—see also Ref. 36. Comparison of accurate DMC calculations for (i) the full problem,³⁴ (ii) an intermediate case in which the ^4He atoms were confined to a sphere, and (iii) the BOAR model itself, provided support that the BOAR approximation captures much of the essential physics, including the turnaround in the effective moment of inertia.³⁵ By further modeling the system as a stirred 1D Tonks-Girardeau (TG) gas³⁷ the existence of a threshold to stirring of the solvent by the dopant molecule was demonstrated, indicative of superfluidity.³⁵ However, that conclusion relied on assuming that the molecule had *already* decoupled adiabatically from the solvent; that is, the molecule was perturbing the solvent but not vice versa. The details of how the molecule decouples were, therefore, not fully elucidated.

Here we study the decoupling mechanism in the BOAR model in more detail and make an explicit connection with the Lieb-Liniger (LL) model of a one-dimensional (1D) quantum gas.³⁸ The TG gas is the hard core limit of the LL model. The main advantage of the BOAR model is that quantum variational calculations are possible and we can follow the quantum behavior directly. This essentially molecular point of view allows us to compute many-body wave functions and avoids the need for phenomenological estimates of superfluid versus normal fluid fractions as is typically done in PIMC calculations.^{39–41} We find that, in the BOAR model, the CO molecule decouples quite early from the ^4He atoms with the system rapidly undergoing a transition to something resembling a Lieb-Liniger (LL) gas. In some ways this situation is similar to a pinning quantum phase transition in which the relative importance of competing terms in the Hamiltonian changes at a critical value.^{42,43}

The article is organized as follows. Section II introduces the BOAR model Hamiltonian and explains the various approximations made, the symmetrization of the basis vectors, and the variational procedure. Section II also discusses the structure of the Hamiltonian matrix which is key to understand the decoupling mechanism with increasing N . In Sec. III the LL and stirred TG (STG) models are introduced and a comparison is made with numerical results obtained in the BOAR model. Conclusions are in Sec. IV where the case of fermionic ^3He clusters is briefly considered.

II. BOSONS-ON-A-RING MODEL

In the BOAR model³⁵ the ^4He atoms are confined to revolve on a ring of radius R_0 measured from the center-of-mass of a linear molecule. The center-of-mass of the molecule is pinned at the origin and the molecule rotates in the plane of the ring.

A. Hamiltonian

The BOAR Hamiltonian is

$$\hat{H} = \frac{\hat{j}_z^2}{2I} + \sum_{\mu=1}^N \left[\frac{\hat{\ell}_\mu^2}{2mR_0^2} + V(\phi_\mu - \theta) \right] + \sum_{\mu < \kappa}^N U(\phi_\mu - \phi_\kappa), \quad (1)$$

where I is the moment of inertia of the molecule and \hat{j}_z is the molecular rotational angular momentum (AM) operator (with quantum number j); the quantity $\hbar^2/2mR_0^2 \text{ cm}^{-1}$ is used to define an effective moment of inertia $I_0 = mR_0^2$ associated with the ^4He atoms; $\hat{\ell}_\mu$ is the orbital AM operator (with quantum number ℓ_μ) for the μ th ^4He atom (mass m), and ϕ_μ and θ are the angles shown in Fig. 1. The atom-molecule intermolecular potential energy surface (PES) is $V(\phi_\mu - \theta)$. The PES⁴⁴ has the radial Jacobi coordinate held fixed, that is, $R = R_0$. We chose $R_0 = 9$ a.u. based on DMC calculations for the full Hamiltonian. The ^4He - ^4He PES is $U(\phi_\mu - \phi_\kappa)$. Two reference angular frequencies are introduced: $\omega_0 = \hbar/I_0$ and $\omega = \hbar/I$. In terms of these quantities the Hamiltonian becomes

$$\begin{aligned} \hat{H} = & -\hbar \omega \frac{\partial^2}{\partial \theta^2} - \hbar \omega_0 \sum_{\mu=1}^N \frac{\partial^2}{\partial \phi_\mu^2} + \sum_{\mu=1}^N V(\phi_\mu - \theta) \\ & + \sum_{\mu < \kappa}^N U(\phi_\mu - \phi_\kappa). \end{aligned} \quad (2)$$

To investigate the effects of the symmetry and strength of the PES, $V(\phi_i - \theta)$ is expanded in Legendre polynomials as follows:

$$V(\Theta_\mu) = \sum_{\lambda=0}^{\lambda=n} V_\lambda(R_0) P_\lambda(\cos \Theta_\mu), \quad (3)$$

where the Jacobi angle $\Theta_\mu = \phi_\mu - \theta$. The V_λ are referred to as radial strength functions. Since we are mainly interested in drawing qualitative conclusions about the decoupling mechanism we set $n = 2$ in Eq. (3) (the strength functions for $n > 2$ are generally relatively small in magnitude). The V_0 strength function provides a constant energy shift and so can be omitted in the BOAR model; however, we retain it for ease of comparison with DMC calculations.

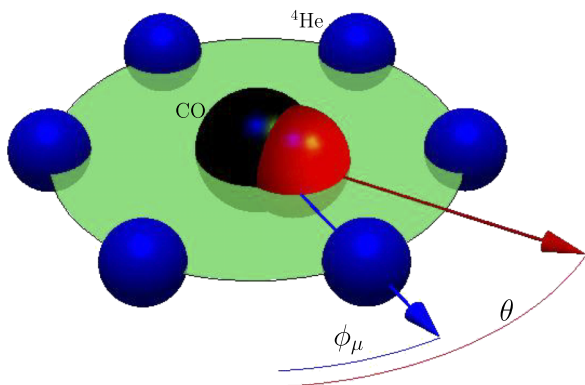


FIG. 1. Bosons on a ring model showing the CO molecule, several ^4He atoms, (not to scale) and their respective angles, θ and ϕ_μ .

TABLE I. Convergence of the lowest energies in the $J = 0$ and $J = 1$ manifolds as a function of j^{max} and ℓ^{max} for $N = 3$. The excited states correlate with the a -type series of energies observed experimentally.³⁰

ℓ^{max}	j^{max}	$E_{J=0} \text{ (cm}^{-1}\text{)}$	$E_{J=1} \text{ (cm}^{-1}\text{)}$
10	0	-18.5283	-17.9194
10	5	-19.5293	-19.3887
10	10	-19.5293	-19.3887
18	0	-18.5285	-17.9201
18	9	-19.5313	-19.3917
18	18	-19.5313	-19.3917
22	0	-18.5286	-17.9203
22	11	-19.5317	-19.3923
22	22	-19.5317	-19.3923

B. ^4He - ^4He interaction

The most accurate ^4He - ^4He PES is that of Aziz *et al.*,⁴⁵ which resembles a Morse potential, and contains an attractive and a repulsive branch. The main difficulty in using this form of PES in a variational study relates to the strong interatomic repulsion when ^4He atoms μ and κ approach each other closely. This complicates the calculation of matrix elements of the potential energy. Therefore we replace the PES by a gaussian barrier on the ring of the form

$$U(\phi_{ij}) = \frac{g}{\sigma\sqrt{2\pi}} e^{-\phi_{\mu\kappa}^2/2\sigma^2}, \quad (4)$$

where $\phi_{\mu\kappa}$ is the angle between ^4He atoms μ and κ . Previous DMC calculations for this Hamiltonian (and also for its analog wherein the atoms are confined to a sphere with the molecule pinned at the center and free to rotate in 3D) have shown that this PES provides good qualitative agreement with experimental results.³⁵ The advantage of using this PES is that (i) the required matrix elements can be easily computed and (ii) the PES has a δ -function as a limit which facilitates

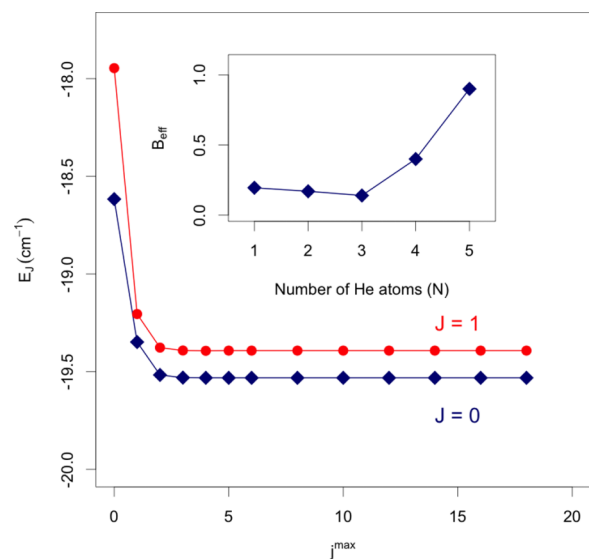


FIG. 2. Convergence of the lowest energies in the $J = 0$ and $J = 1$ manifolds as a function of j^{max} with $\ell^{\text{max}} = 18$ for $N = 3$. The $J = 1$ state corresponds to the experimentally probed a -series of states. The inset shows B_{eff} as a function of N .

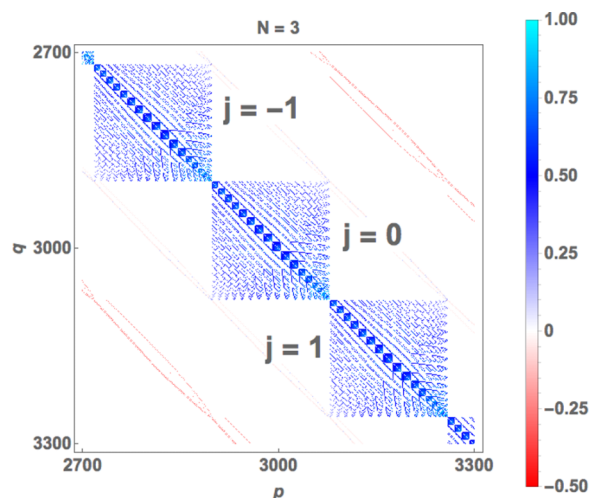


FIG. 3. Plot of part of the Hamiltonian matrix—shown as $\log_{10}(|H_{pq}|)$ —with $N = 3$ and $j^{\max} = \ell^{\max} = 18$. The large central blocks have fixed values of j and arise from the diagonal parts of the Hamiltonian and the ${}^4\text{He}$ - ${}^4\text{He}$ interaction. The elements outside of the blocks arise from the molecule- ${}^4\text{He}$ atom interactions.

comparison with the LL and TG models. Throughout we set $\sigma = 0.1 \text{ rad}^{-1}$ and $\frac{g}{\sigma\sqrt{2\pi}} = 75 \text{ cm}^{-1}$. These values were chosen to make a rough match with the onset of the repulsive wall of the accurate potential. Varying these values affects the details

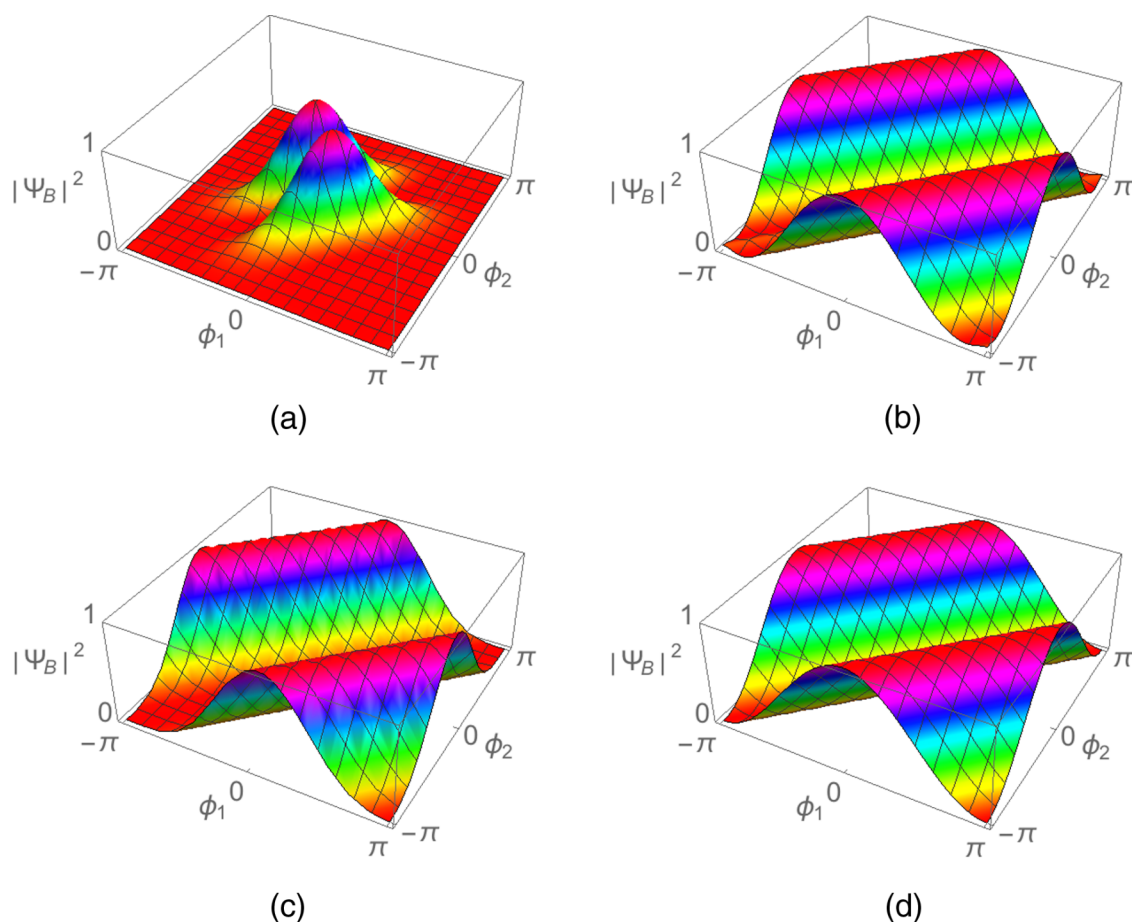


FIG. 5. Projections of ground state probability densities for $N = 2$ with $\theta = 0$ obtained using: (a) the accurate BOAR wave function, (b) the BOAR wave function with the molecule omitted, and (c) the Lieb-Liniger wave function. For clarity the vertical axes were scaled to the interval $(0, 1)$.

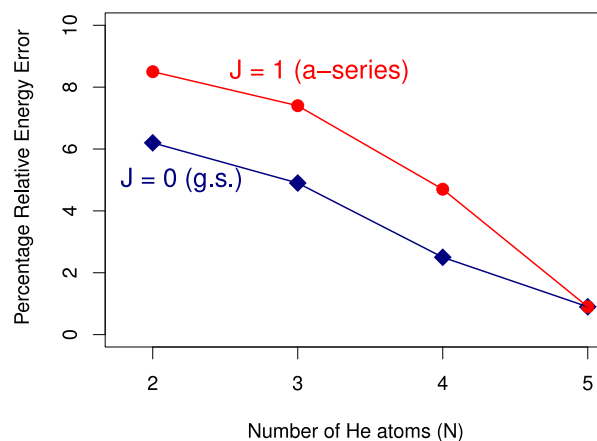


FIG. 4. Percentage relative error in energy as obtained using only a single block ($j^{\max} = 0$) as a function of the number of ${}^4\text{He}$ atoms (N) with $\ell^{\max} = 18$. The energies are the lowest in the $J = 0$ and $J = 1$ manifolds.

somewhat but, provided the value of g is sufficiently large, the qualitative picture is unaffected.

C. Basis set calculations

The Hamiltonian of Eq. (1) is diagonalized using the Lanczos algorithm⁴⁶ in a symmetrized basis built from the following product *primitive* basis functions for N ${}^4\text{He}$ atoms:

$$\psi_{j,\{\ell_\mu\}} = \left(\frac{1}{\sqrt{2\pi}}\right)^{N+1} e^{i(j\theta)} \prod_{\mu=1}^N e^{i\ell_\mu\phi_\mu}. \quad (5)$$

The quantum numbers are allowed to range between specified maximum and minimum values; $(-j^{\max} \leq j \leq j^{\max})$ and $(-\ell^{\max} \leq \ell_\mu \leq \ell^{\max})$. The symmetrized basis vectors (SBVs) are linear combinations of primitive basis vectors containing all permutations of their ℓ_μ quantum numbers. The total angular momentum of the system, J , given by

$$J = j + \sum_{\mu=1}^N \ell_\mu = j + L \quad (6)$$

is conserved. The SBVs are conveniently organized by the quantum number j which introduces an almost block-diagonal structure into the Hamiltonian matrix. The number of primitive basis vectors grows rapidly with the number of ^4He atoms and also with the magnitude of j^{\max} and ℓ^{\max} . For example, with $N = 4$ and $j^{\max} = \ell^{\max} = 18$ there are 1 122 901 primitive basis vectors and the Hamiltonian matrix is $53\,088 \times 53\,088$. For $N = 5$ with the same values of j^{\max} and ℓ^{\max} there are 38 151 847 primitive basis vectors and the Hamiltonian matrix is $395\,152 \times 395\,152$.

In principle, j^{\max} and ℓ^{\max} need not necessarily span the same ranges in order to obtain convergence. Therefore, we investigated convergence of both the eigenvalues and eigenvectors as a function j^{\max} and ℓ^{\max} separately. Table I shows the convergence behavior of the lowest eigenvalues

in the $J = 0$ and $J = 1$ manifolds as a function of j^{\max} and ℓ^{\max} for $N = 3$. The situation is similar for other values of N . Also shown in Fig. 2 is the convergence of the lowest $J = 0$ and $J = 1$ levels as a function of j^{\max} with $\ell^{\max} = 18$. These energy levels were chosen because they are the ones accessed in recent experiments. Two overall trends are clear: (i) for a given ℓ^{\max} , convergence as a function of j^{\max} is quite rapid and (ii) for a sufficiently large j^{\max} (typically in the range 6–8) overall convergence requires a relatively larger value of ℓ^{\max} , typically in the range 12–18.

This convergence behavior is supported by the fact that the eigenvalues of a symmetric matrix are well conditioned, that is, they are slightly affected by small perturbations of the original matrix.⁴⁷ Even more, the matrix can be brought into a more convenient form by adding a sufficiently large quantity to the whole diagonal in such a way that it becomes strictly row diagonal dominant. For this type of matrix useful results about the bounds of the eigenvalues exist.^{48,49} Indeed, if we introduce the diagonally dominant part of a row of a given matrix as

$$v_i = a_{ii} - \sum_{j \neq i} a_{ij},$$

the relative error for the eigenvalues can be bounded by ϵ , if it is less than unity and it is verified

$$|v_i - \tilde{v}_i| \leq \epsilon |v_i|,$$

being v_i and \tilde{v}_i the diagonally dominant parts of the given matrix and the close one. We note that this bound is not

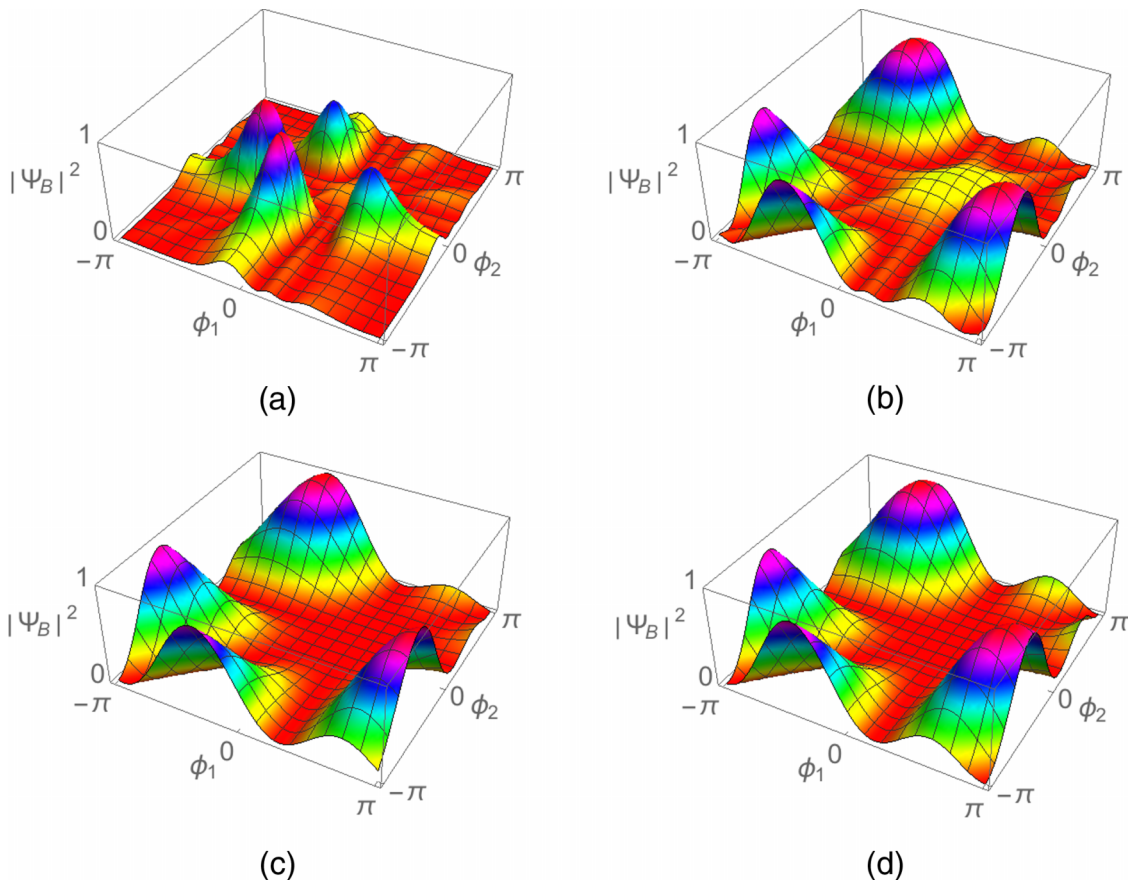


FIG. 6. Projections of ground state probability densities for $N = 3$ with $\theta = 0$ and $\phi_3 = \pi/5$ obtained using (a) the accurate BOAR wave function, (b) the BOAR wave function with the molecule omitted, (c) the Lieb-Liniger wave function, and (d) the Tonks-Girardeau wave function. For clarity the vertical axes were scaled to the interval (0,1).

good enough if $\epsilon \approx 1$. However, in our case, the approximated matrices are constructed step by step. In the first step the approximated matrix is block diagonal, so that the eigenvalues are those of the blocks. As the lowest eigenvalue belongs to the central block, this is our first estimation. In the second step, we add the off diagonal-block elements coupling the three central blocks. Once again, the lowest eigenvalue corresponds to the coupled central three blocks. In the next step we consider the coupling elements for the five central blocks and so on. In each step, the trace of the matrix is conserved and, due to the interlacing property⁴⁷ and the previous bound, we get a good accuracy for the lowest eigenvalue after three or four steps.

These observations allow some computational simplifications to be made for larger values of N . They also provide insight into the decoupling mechanism. It should be noted that the value of ℓ^{\max} necessary for acceptable convergence increases as the gaussian ^4He - ^4He interaction becomes narrower. In the LL limit of a δ -function very large values of ℓ^{\max} are necessary to achieve even acceptable convergence, as has been noted previously.⁵⁰

While it is apparent from Table I that, for a given value of ℓ^{\max} , convergence as a function of j^{\max} is quite rapid, relatively large values of ℓ^{\max} are needed to ensure final convergence. This conclusion is similar for other values of N and can be understood by examining the structure of the Hamiltonian matrix which is shown in Fig. 3 for $N = 3$. The main conclusion is that the molecule- ^4He interactions lie away from the diagonal

and are relatively small in comparison to the atom-atom interactions which have a block diagonal structure. Crucially, each of the blocks conserves the value of j because the atom-atom interaction potential does not couple directly to the molecule. That is, in the absence of atom-molecules interactions (or for an isotropic PES) the quantum number j would be exactly conserved, i.e., it would be a good quantum number. Because j is conserved within each block this is a measure of how strongly coupled the molecule is to the ^4He atoms in comparison to ^4He - ^4He interactions. Figure 4 shows the percentage of the converged energy recovered by including only a single block, i.e., the $j = 0$ block for the ground and also the a -type series of the CO - $^4\text{He}_N$ complex. It is clear that, with increasing N , convergence accelerates which indicates that fewer blocks are needed. In turn this suggests increasing decoupling.

If the molecule is assumed to have decoupled completely then the BOAR Hamiltonian is quite similar to that for an important 1D problem, the Lieb-Liniger gas.^{38,50,51}

III. REDUCED DIMENSIONALITY MODELS

A. Lieb-Liniger model

The Lieb-Liniger (LL) Hamiltonian can be used to describe a system of N spinless, repulsive bosons confined to a ring.^{7,38} In dimensionless coordinates x_μ with $0 \leq x_\mu \leq L$ where L is the (dimensionless) length of the ring the

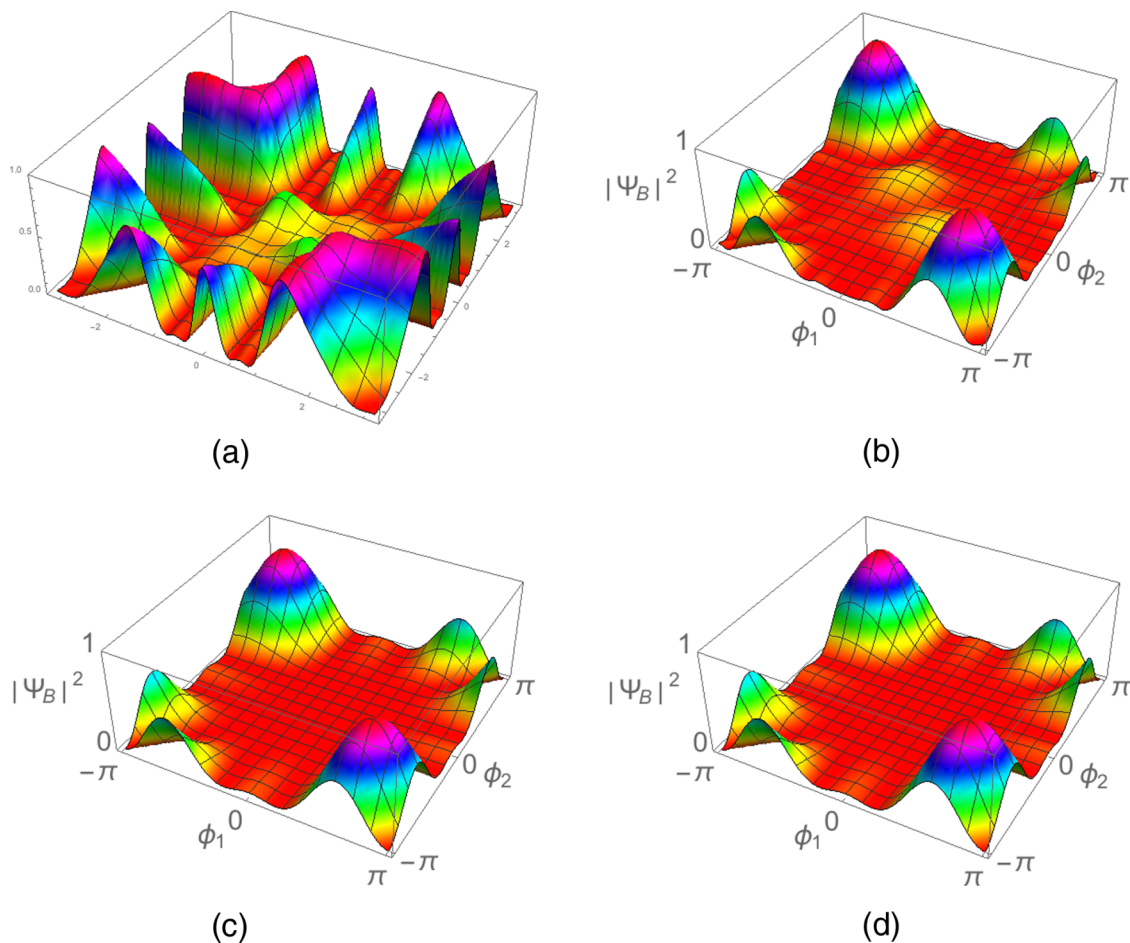


FIG. 7. As for Fig. 5 with $N = 4$. Here $\phi_3 = \pi/5$ and $\phi_4 = -\pi/5$.

Hamiltonian is given by

$$\hat{H} = -\frac{\hbar^2}{2m} \sum_{\mu=1}^N \frac{\partial^2}{\partial x_{\mu}^2} + g_{1D} \sum_{\mu < \kappa}^N \delta(x_{\mu} - x_{\kappa}). \quad (7)$$

Here m is the mass of each boson and the interaction potential is a δ -function where g_{1D} measures its strength. The bosons are repulsive for $g_{1D} > 0$ and attractive when $g_{1D} < 0$. Only the repulsive case is considered here.

The LL model reduces to $N - 1$ coupled transcendental equations that can be solved to yield the exact N -particle ground state. Lieb and Liniger solved this problem but only considered the $N = 2$ case and the thermodynamic limit in detail. Recently, Cederbaum and co-workers have obtained accurate LL solutions up to $N = 50$.⁵⁰ The reason for considering the LL model is that it corresponds to the BOAR model in which the molecule is completely decoupled, albeit with a δ -function, rather than a gaussian, interaction. The quantity g_{1D} was chosen so that, in the limit $\sigma \rightarrow 0$, the gaussian in the BOAR model tends to the corresponding δ -function limit.

The *unnormalized* LL wave functions obtained using the Bethe-ansatz^{38,52} are given by

$$\psi = \sum_P a(P) P \exp\left(i \sum_{\mu=1}^N k_{\mu} x_{\mu}\right), \quad (8)$$

where k_{μ} are wave vectors and the sum is over all permutations, P , of the $\{x_{\mu}\}$. The coefficients $a(P)$ are obtained as described in Refs. 38, 50, and 53; briefly, if $P = I$, the identity, then $a(I) = 1$. Otherwise P is decomposed into transpositions, and for every transposition of particles μ and κ , a factor, $-e^{i\Omega_{\mu\kappa}}$ is generated with $\Omega_{\mu\kappa}$ defined below. The coefficient $a(P)$ is the product of these factors. The $\{k_{\mu}\}$ can then be obtained as the solutions to the following set of transcendental equations:⁵⁰

$$k_{\mu}L = 2\pi I_{\mu} - \sum_{n=1}^N \Omega_{n\mu}, \quad \mu = 1, 2, \dots, N, \quad (9)$$

where

$$\Omega_{\mu\kappa} = i \ln \left[\frac{c + i(k_{\mu} - k_{\kappa})}{c - i(k_{\mu} - k_{\kappa})} \right] = -2 \arctan \left(\frac{k_{\mu} - k_{\kappa}}{c} \right), \quad (10)$$

where $c = g_{1D}/2$ and the $\{I_{\mu}\}$ are a set of integers when N is odd and are half-integers when N is even. For the ground state the $\{I_{\mu}\}$ are defined by

$$I_{\mu+1} - I_{\mu} = 1, \quad 1 \leq \mu < N \quad \text{and} \quad I_1 = -I_N. \quad (11)$$

Two sets of excitations exist labeled type I and type II by Lieb.⁵¹ We only consider particle excitations which correspond to type I excitations and are obtained by defining $I_1 \dots I_{N-1}$ as for the ground state but increasing I_N by a positive integer. Alternatively, one may keep $I_2 \dots I_N$ as for the ground state but decrease I_1 by a positive integer. Although the system of

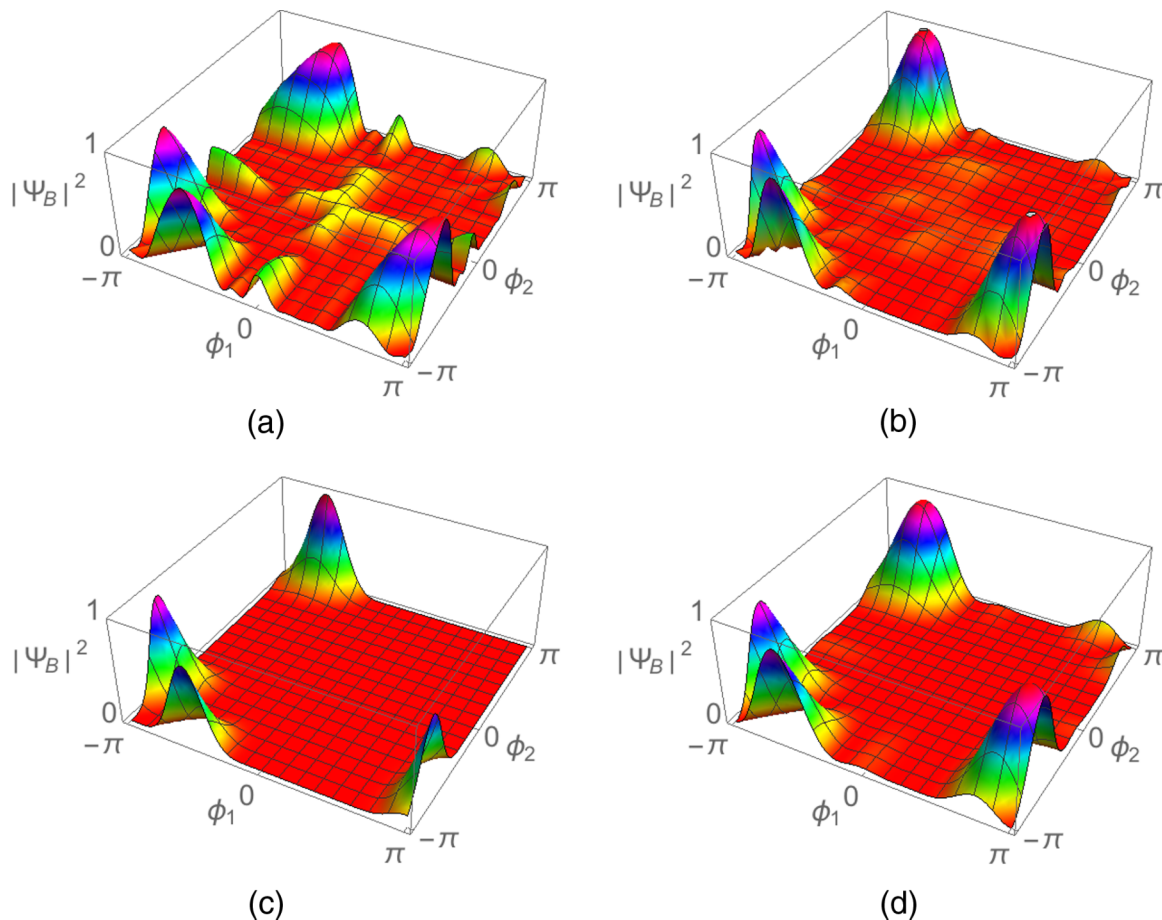


FIG. 8. As for Fig. 6 with $N = 5$. Here $\phi_3 = \pi/5$, $\phi_4 = -\pi/5$ and $\phi_5 = 2\pi/5$.

equations described by Eq. (9) can be solved algebraically, this becomes increasingly complicated with increasing N . However, it is straightforward to solve them numerically, in this case using a genetic algorithm. Comparison with exact results available online⁵⁴ demonstrates the accuracy of this method. Mathematica⁵⁵ was used to generate and plot the LL eigenfunctions using the numerically obtained values of the $\{k_\mu\}$.

Figures 5–8 show projections of the BOAR probability densities, with and without the atom-molecule interaction together with the accurate LL probability density. For comparison the TG probability density is also shown. It is apparent that, with increasing N , the BOAR case is tending to the LL limit which is indicative of molecule-solvent decoupling. The BOAR plots without the atom-molecule interaction included are, in all cases, very similar to the LL model and this serves as a test of the convergence of the variational calculations. This is important because of the difficulty in converging the LL problem by direct diagonalization of the Hamiltonian.⁵⁶ The good agreement observed indicates reasonable convergence of the wave function (with the caveat that the BOAR model uses a gaussian rather than a δ -potential). Because the wave functions are multidimensional, in making the plots, we fixed the angles of all but two of the ^4He atoms. Our general conclusions are not sensitive to the particular values of these angles. Figure 9 is a similar plot for the lowest $J = 1$ excited state with $N = 3$. This state correlates with the

uncoupled state $|j, \ell_1, \ell_2, \ell_3\rangle = |0, 1, 0, 0\rangle$ (and its symmetric permutations over the ^4He atoms) and is part of the a -type series of transitions observed experimentally.³¹ Again, the good agreement between the BOAR model without the molecule and the LL result suggests good convergence of our calculations for the excited states of interest.

The evolution of the system to the LL limit with increasing N is a clear indicator of molecule-solvent decoupling. However, these results also predict that decoupling will be sensitive to (i) the size of the rotational constant, B_0 and (ii) the strength of the molecule-atom interaction potential. To confirm this we computed wave functions using nonphysical values for B_0 and also varied the size of the radial strength functions in Eq. (3). Figure 10 compares probability densities for $N = 3$ with the “fudged” rotational constant B_f set to $10B_0$ and $B_0/10$ while using the physical values for V_1 and V_2 in Eq. (3). For the larger value of B_f the plot is almost identical to Fig. 6(b) ($N = 3$, no molecule present); that is the increased rotational constant leads to faster decoupling. The nonphysical, larger value of B_f is causing the intermolecular potential to appear to be essentially isotropic. In contrast, with the reduced value of B_f the system lies further away from the uncoupled (LL) limit; that is later decoupling is observed. Stated differently, the amount of “adiabatic following”¹⁷ is reduced (increased) by increasing (reducing) B_f . This effect also depends on the strength of the intermolecular potential. Figure 10(c) illustrates this; it shows the result obtained when the values of V_1 and V_2 are tripled while setting

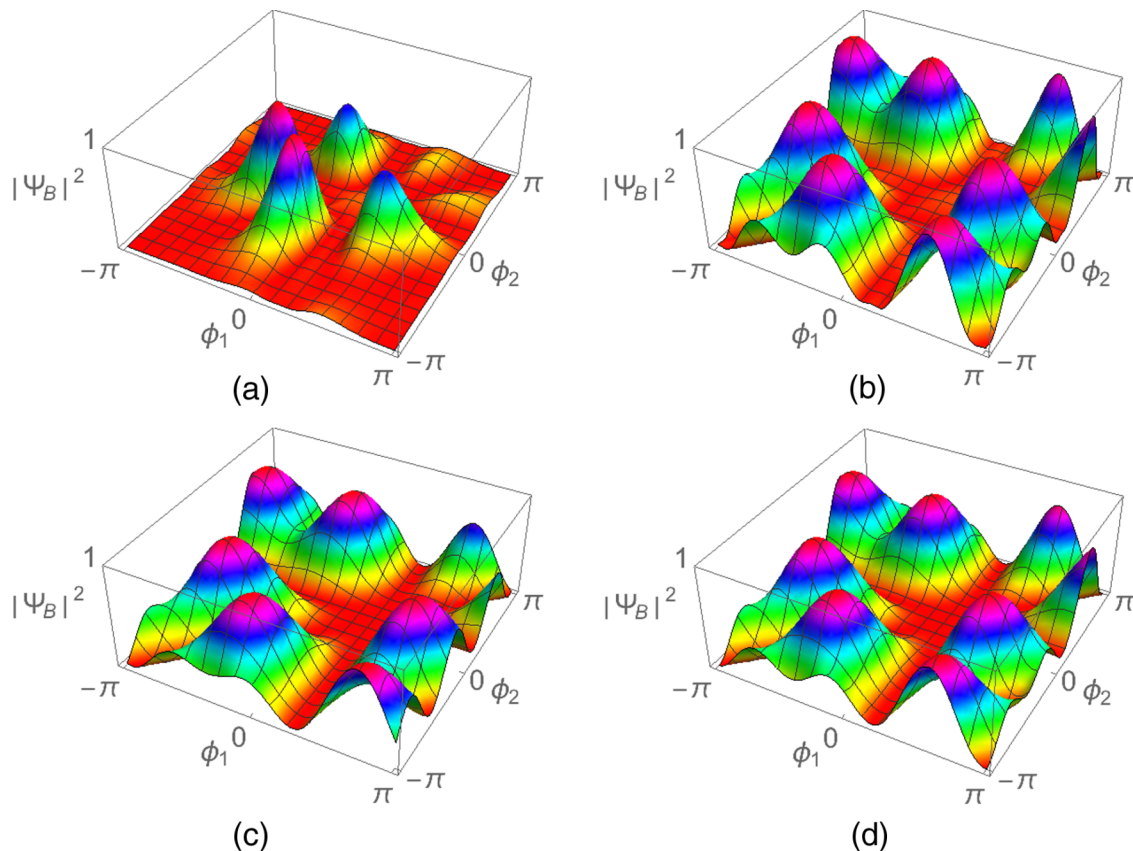


FIG. 9. Projections of the first $J = 1$ excited state probability density with $N = 3$, $\phi_3 = \pi/5$, and $\theta = 0$ obtained using: (a) the accurate BOAR wave function, (b) the BOAR wave function with the molecule omitted, (c) the Lieb-Liniger wave function, (d) the TG wave function. For clarity the vertical axes were scaled to the interval (0,1).

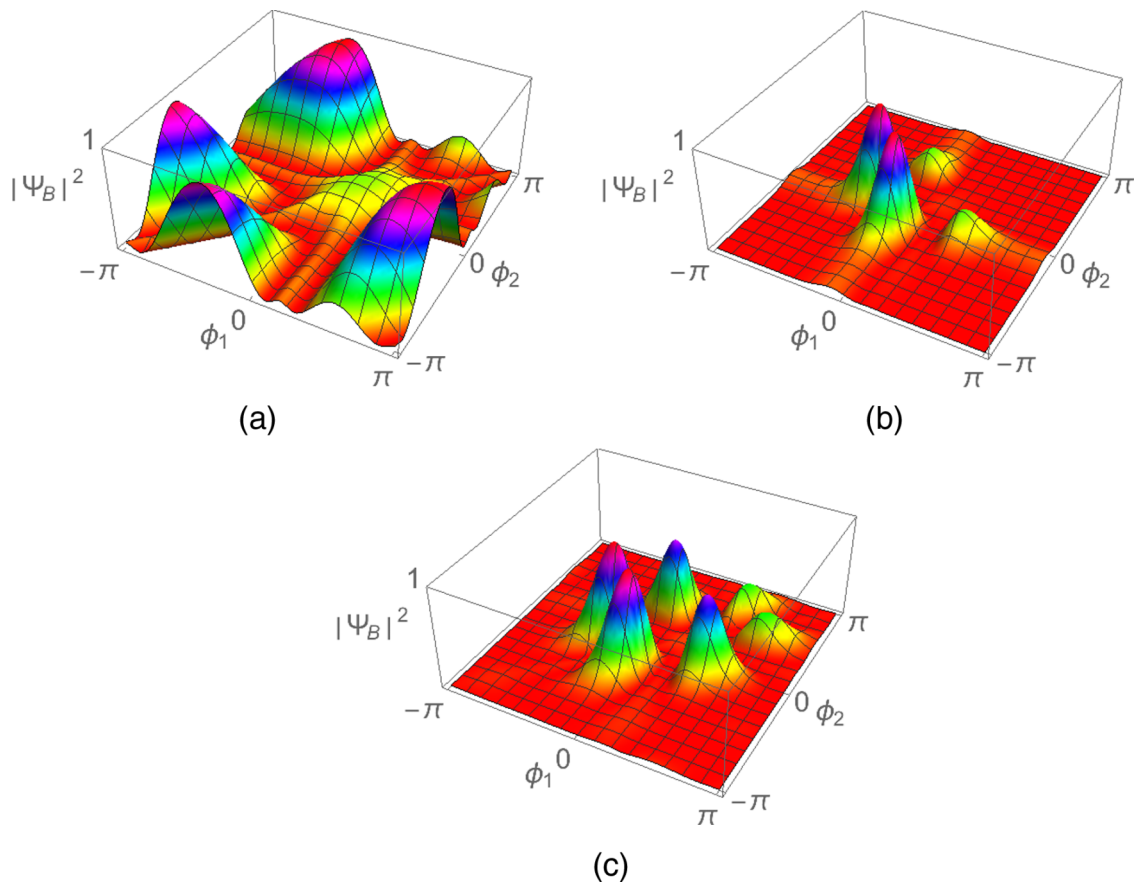


FIG. 10. Projections of the ground state probability density with $N = 3$, $\phi_3 = \pi/5$, and $\theta = 0$. (a) $B_f = 10B_0$; (b) $B_f = B_0/10$; (c) $B_f = 10B_0$ and with V_1 and V_2 taking values 3 times their physical values. For clarity the vertical axes were scaled to the interval (0,1).

$B_f = 10B_0$. In this case the effect of increasing B_f in Fig. 10(a) has been almost nullified by increasing the strength of the potential.

It is also interesting to examine the effect of changing the strength of the ${}^4\text{He}$ - ${}^4\text{He}$ repulsion. Figure 11 shows the probability density when g in Eq. (4) is reduced by a factor of 15. In this case the ${}^4\text{He}$ density piles on to the end of the molecule, that is, the molecule-atom interaction dominates the very weak repulsive interatomic potential. This means that decoupling will occur much later, if at all. In

agreement with this, the LL limit, also shown, is markedly different.

The situation is similar to a pinning quantum phase transition in which the relative importance of competing terms in the Hamiltonian changes at a critical value.^{42,43} As N increases and passes a critical value this ordering is reversed. The results so far suggest that the LL model introduced previously lies rather close to the TG limit.³⁵ Therefore we model the problem as a stirred TG gas, for which the wave functions are much simpler than in the LL case.

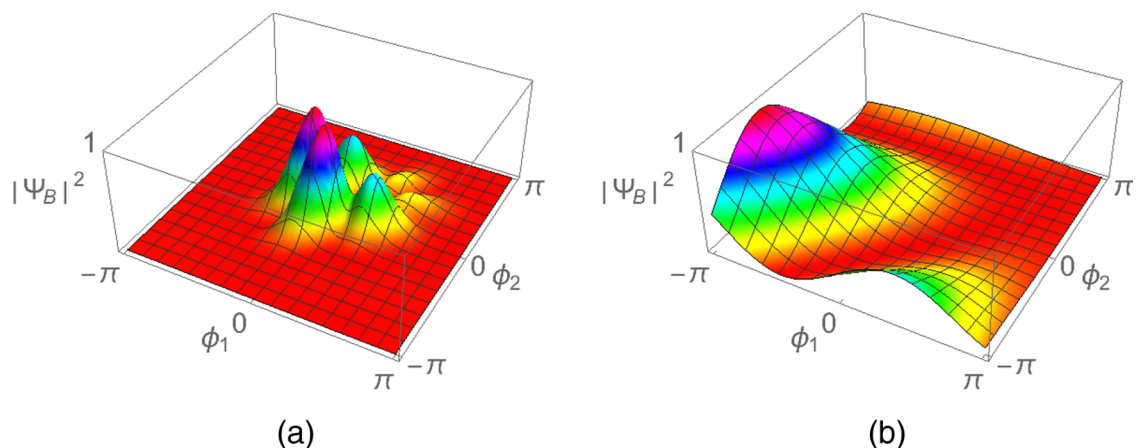


FIG. 11. Projections of the ground state probability density with $N = 3$, $\phi_3 = \pi/5$, and $\theta = 0$ and with g reduced by a factor of 15. (a) BOAR (b) LL. For clarity the vertical axes were scaled to the interval (0,1).

B. Stirred Tonks-Girardeau gas

The TG Hamiltonian is the $g_{1D} \rightarrow \infty$ limit of Eq. (7).^{37,50} The TG ground state wave function for an odd number $N \geq 3$ of bosons is³⁷

$$\psi_0^B = |\psi_0^F| = \frac{1}{\sqrt{N!L^N 2^{N(N-1)}}} \prod_{\mu > \kappa} |\sin[\frac{\pi}{L}(\phi_\mu - \phi_\kappa)]| \quad (12)$$

with energy

$$E_0 = \frac{1}{6}(N - \frac{1}{N}) \frac{(\pi \hbar N)^2}{mL^2}. \quad (13)$$

Examples of TG ground state probability densities are shown in Figs. 6 and 8 and are similar to the LL results. For even N the situation is somewhat more complicated and we do not consider it here. The lowest excited state wave function is³⁷

$$\psi_1^B = \psi_0^B \sum_{\mu=1}^N e^{2\pi i \phi_\mu / L} \quad (14)$$

with energy $E_1 = E_0 + \epsilon_{k_1}$ where $k_1 = 2\pi/L$ and

$$\epsilon_{k_1} = \frac{\hbar^2}{m} k_1 \left[\frac{(N-1)\pi}{L} + \frac{1}{2} k_1 \right]. \quad (15)$$

The states are actually doubly degenerate because of the two senses of angular momentum in the ring but here we consider only excitations in the positive sense. Figure 9(d)

shows a projection of the lowest TG excited state probability density which agrees well with the LL limit. This suggests diagonalizing the following Hamiltonian for a TG gas (with $g \rightarrow \infty$) stirred by the molecule.³⁵

$$\hat{H}_{\text{STG}} = -\hbar \omega \frac{\partial^2}{\partial \theta^2} - \hbar \omega_0 \sum_{\mu=1}^N \frac{\partial^2}{\partial \phi_\mu^2} + g \sum_{\mu < \kappa}^N \delta(\phi_\mu - \phi_\kappa) + \sum_{\mu=1}^N V(\phi_\mu - \theta). \quad (16)$$

To simplify the model even further we use a direct product basis consisting only of the ground and lowest excited TG states combined with the $j = 0, \pm 1$ states of the molecule. In this notation the state $|10\rangle$, for example, corresponds to the wave function $e^{i\theta} \psi_0^B$ for each N . In the intermolecular potential we include only the terms in V_1 , i.e., the intermolecular potential used here is $\mathcal{V} = V_1 \sum_{\mu}^N \cos(\phi_\mu - \theta)$. The diagonal elements of the Hamiltonian in this very reduced basis are $E_0 + B_0 j(j+1)\hbar^2$ and $E_1 + B_0 j(j+1)\hbar^2$. The additive rotational energy of the molecule is independent of N and so the diagonal terms grow as N^3 —see Eqs. (13) and (15). By symmetry, only states with $\Delta j = \pm 1$ can be coupled by \mathcal{V} which gives rise to off-diagonal matrix elements. In this basis the non-zero off-diagonal matrix elements have the form [using Eq. (15)], for example,

$$\begin{aligned} \langle 00 | \mathcal{V} | 11 \rangle = & V_1 \sum_{\mu=1}^N \left[\langle 0 | \cos \theta | 1 \rangle \times \int_0^{2\pi} d\phi_1 \dots \int_0^{2\pi} d\phi_N |\psi_0^B|^2 \times \left(\sum_{\kappa=1}^N e^{2\pi i \phi_\kappa / L} \right) \cos \phi_\mu \right. \\ & \left. + \langle 0 | \sin \theta | 1 \rangle \times \int_0^{2\pi} d\phi_1 \dots \int_0^{2\pi} d\phi_N |\psi_0^B|^2 \times \left(\sum_{\kappa=1}^N e^{2\pi i \phi_\kappa / L} \right) \sin \phi_\mu \right]. \quad (17) \end{aligned}$$

For relatively small N these integrals can be done analytically using Mathematica⁵⁵ and we find that they are constant as a function of N —this was verified up to $N = 7$. Thus the diagonal matrix elements rapidly dominate the off-diagonal elements as N increases, in accord with our earlier numerical findings. That is, the molecule rapidly decouples from the solvent as N grows larger.

IV. CONCLUSIONS

Microscopic superfluidity has been proposed as the reason that the effective moments of inertia of many molecules in ⁴He droplets start a nonclassical decrease as the number of solvent atoms is increased. Spectra reveal that the molecule undergoes apparent frictionless free rotation, but with spectroscopic constants different from their gas phase values. These observations, combined with the direct observation of superfluidity in recent experiments,^{19,20} and PIMC calculations, make for a compelling case that these systems are superfluid.

To further address this question, and motivated by previous accurate DMC calculations for CO-⁴He_N complexes,

we introduced a reduced dimensionality model in which the atoms are confined to a ring. The boson-boson interaction was modeled as a repulsive gaussian barrier. Variational and previous DMC calculations demonstrated that the observed turnaround in the effective rotational constant is captured qualitatively by this model, which suggests that the underlying physics is similar to the full-dimensionality problem.

The LL model provides an analytically soluble limit for the BOAR model of N bosons confined to a ring but with the molecule absent. Thus, by comparing the wave functions of the BOAR and LL models it was possible to gauge the degree to which the molecule had decoupled from the solvent. In the BOAR model the point at which decoupling starts to occur depends on the rotational constant of the molecule, the strength of the intermolecular potential, and the number and strength of the repulsive interactions between the bosons. In the LL model the energy splitting between the ground and lowest excited state increases with N , that is, as more atoms are confined to the ring. The competition between this tendency to increase the energy splitting and the molecule-atom interaction, which tends to decrease this energy splitting (by increasing the

effective moment of inertia of the molecule) is what leads to a turnaround in the effective rotational constant. This is consistent with the experimental observation that different molecules begin the decoupling process at different values of N . In part, this is related to the size of their rotational constants and to the strength and symmetry of the intermolecular potential.²⁶ Naturally, at some point the ring will become too crowded and the BOAR model will break down. For some molecules, e.g., N_2O and OCS , the 4He atoms do initially inhabit a ring but around the *waist* of the molecule, that is, the axis of the molecule is perpendicular to the plane containing the atoms (in contrast to Fig. 1). Applying the BOAR model to this geometry would lead to no turnaround at all because the intermolecular potential is isotropic for bosons strictly confined to a ring in this configuration. Also, for heavier bosons (e.g., bosonic Ne) no turnaround is expected because of the much stronger intermolecular potential as compared to typical 4He -molecule interactions. In addition, attractive interactions between solvent bosons, ignored here, will play a more important role. Already for bosonic $p-H_2$ clusters the attractive interactions are somewhat stronger than for 4He atoms; however, comparable behavior to $CO-(p-H_2)_N$ clusters is observed which suggests a similar mechanism (except for the behavior of the rotational constant in the nanodroplet limit). PIMC calculations also show that these clusters are superfluid.³¹

The Bose symmetry requirement places constraints on the 4He - 4He part of the wave function which tends to its ground angular momentum state as more atoms are added. That is the $J = 0$ ground state eventually becomes the one in which $j = 0$ and $L = \sum_i \ell_i = 0$ separately, i.e., j and L become “almost-good” quantum numbers. As noted by Girardeau,³⁷ in a 1D TG gas, fermions will behave in the same manner as bosons. Therefore the 1D BOAR model does not distinguish between 4He and 3He in terms of atomic statistics. The situation will be different if the atoms are not confined to 1D because of the Pauli exclusion principle which is expected to lead to significant coupling between j and L for 3He . For example, we expect that a difference will quickly become apparent between 3He and 4He if the bosons are confined to a sphere. It is worth pointing out that recent experimental and theoretical studies of small OCS - 3He_N clusters find, somewhat surprisingly, that the rotational features in 3He clusters are quite similar to 4He droplets, although considerably broadened.^{57,58}

Our conclusions based on numerical results were strengthened by considering the case of a TG gas stirred by a molecule. As the number of solvent atoms increases, the coupling matrix elements between the molecule and the solvent atoms diminish rapidly in comparison to boson-boson interactions. That is, the decoupling of the molecule can be explained entirely in terms of the Schrödinger equation without explicit resort to the notion of superfluidity—although that is not to say that these systems are not superfluid. We also note recent density functional calculations that report a quantum phase transition^{59,60} between a localized state and an intermediate 1D superfluid⁶¹ along the way to bulk superfluidity. This transition involves particle-hole excitations and is consistent with earlier findings using the BOAR model³⁵ and this work.

Microscopic superfluidity—signaled by the turnaround in B_{eff} —has, we conclude, its origin in a combination of factors: the unusually weak coupling of the molecule to the solvent, the Bose symmetry of the solvent atom wave function, and the repulsive interactions between the bosons which dominate as N increases. Of course, several of these ingredients are precisely the reason that bulk helium-4 can exist as a superfluid in the first place.

ACKNOWLEDGMENTS

This work was supported, in part, by Grant No. CHE1300504 from the National Science Foundation and Grant Nos. MTM2011-28227-CO-2 and MTM2014-59433-C2 from the Spanish Ministry of Science and Innovation. We thank Dr. Antonio Gamboa for a number of useful suggestions and comments.

- ¹P. Kapitza, “Viscosity of liquid Helium below the λ -point,” *Nature* **141**, 74 (1938).
- ²J. F. Allen and A. D. Misener, “Flow of liquid Helium II,” *Nature* **141**, 75 (1938).
- ³D. Vollhardt and P. Wölfle, *The Superfluid Phases of Helium 3* (Taylor and Francis, London, 1990).
- ⁴U. Lombardo and H. Josef Schulze, “Superfluidity in neutron star matter,” in *Physics of Neutron Star Interiors*, Lecture Notes in Physics Vol. 578 (Springer, 2001), pp. 30–53.
- ⁵P. S. Shternin, D. G. Yakovlev, C. O. Heinke, W. C. G. Ho, and D. Patnaude, “Cooling neutron star in the Cassiopeia A supernova remnant: Evidence for superfluidity in the core,” *Mon. Not. R. Astron. Soc.* **412**, L108–L112 (2011).
- ⁶M. W. Zwierlein, J. Abo-Shaeer, A. Schirotzek, C. H. Schunck, and W. Ketterle, “Vortices and superfluidity in a strongly interacting Fermi gas,” *Nature* **435**, 1047–1051 (2005).
- ⁷D. M. Ceperley, “Path integrals in the theory of condensed helium,” *Rev. Mod. Phys.* **67**, 279–355 (1995).
- ⁸M. Hartmann, F. Mielke, J. P. Toennies, A. F. Vilesov, and G. Benedek, “Direct spectroscopic observation of elementary excitations in superfluid He droplets,” *Phys. Rev. Lett.* **76**, 4560–4563 (1996).
- ⁹M. Hartmann, R. E. Miller, J. P. Toennies, and A. Vilesov, “Rotationally resolved spectroscopy of SF_6 in liquid-helium clusters: A molecular probe of cluster temperature,” *Phys. Rev. Lett.* **75**, 1566–1569 (1995).
- ¹⁰S. Grebenev, J. P. Toennies, and A. F. Vilesov, “Superfluidity within a small helium-4 cluster: The microscopic Andronikashvili experiment,” *Science* **279**, 2083–2086 (1998).
- ¹¹S. Goyal, D. L. Schutt, and G. Scoles, “Vibrational spectroscopy of sulfurhexafluoride attached to helium clusters,” *Phys. Rev. Lett.* **69**, 933–936 (1992).
- ¹²B. S. Dumesht, A. V. Potapov, and L. A. Surin, “Spectroscopy of small helium clusters and ‘nanoscopic’ superfluidity: He_N -CO, $N = 2$ –20,” *Phys.-Usp.* **52**, 294–298 (2009).
- ¹³C. Callegari, K. K. Lehmann, R. Schmied, and G. Scoles, “Helium nanodroplet isolation rovibrational spectroscopy: Methods and recent results,” *J. Chem. Phys.* **115**, 10090–10110 (2001).
- ¹⁴M. Y. Choi, G. E. Douberly, T. M. Falconer, W. K. Lewis, C. M. Lindsay, J. M. Merritt, P. L. Stiles, and R. E. Miller, “Infrared spectroscopy of helium nanodroplets: Novel methods for physics and chemistry,” *Int. Rev. Phys. Chem.* **25**, 15–75 (2006).
- ¹⁵M. Barranco, R. Guardiola, S. Hernández, R. Mayol, J. Navarro, and M. Pi, “Helium nanodroplets: An overview,” *J. Low Temp. Phys.* **142**, 1–81 (2006).
- ¹⁶C. Callegari, W. Jäger, and F. Stienkemeier, “Helium nanodroplets,” in *Handbook of Nanophysics: Nanoparticles and Quantum Dots*, edited by K. D. Sattler (CRC Press Taylor and Francis Group, Boca Raton, FL, 2011), Chap. 4, pp. 4.1–4.28.
- ¹⁷E. Lee, D. Farrelly, and K. B. Whaley, “Rotational level structure of SF_6 -doped 4He_N clusters,” *Phys. Rev. Lett.* **83**, 3812–3815 (1999).
- ¹⁸A. Conjusteau, C. Callegari, I. Reinhard, K. K. Lehmann, and G. Scoles, “Microwave spectra of HCN and DCN in 4He nanodroplets: A test of adiabatic following,” *J. Chem. Phys.* **113**, 4840–4843 (2000).

- ¹⁹N. B. Brauer, S. Smolarek, E. Loginov, A. Hernando, M. Pi, M. Barranco, W. J. Buma, and M. Dravvels, "Critical Landau velocity in Helium nanodroplets," *Phys. Rev. Lett.* **111**, 153002-1–153002-5 (2013).
- ²⁰L. F. Gomez et al., "Shapes and vortices of superfluid helium," *Science* **345**, 906–909 (2014).
- ²¹A. Yu, J.-S. Cherny, and J. Brand, "Theory of superfluidity and drag force in the one-dimensional Bose gas," *Front. Phys.* **7**(1), 54–71 (2012).
- ²²J. Tang, Y. J. Xu, A. R. W. McKellar, and W. Jäger, "Quantum solvation of carbonyl sulfide with helium atoms," *Science* **297**, 2030–2033 (2002).
- ²³A. R. W. McKellar, Y. J. Xu, and W. Jäger, "Spectroscopic exploration of atomic scale superfluidity in doped Helium nanoclusters," *Phys. Rev. Lett.* **97**, 183401-1–183401-2 (2006).
- ²⁴L. A. Surin, "Nonclassical rotations of single molecules in small helium and hydrogen clusters: Manifestation of microscopic superfluidity," *JETP Lett.* **97**, 57–65 (2013).
- ²⁵J. P. Toennies, "Helium clusters: Microscopic superfluidity and other quantum effects," *Mol. Phys.* **111**, 1879–1891 (2013).
- ²⁶L. A. Surin, A. V. Potapov, B. S. Dumesh, S. Schlemmer, Y. Xu, P. L. Raston, and W. Jäger, "Rotational study of carbon monoxide solvated with helium atoms," *Phys. Rev. Lett.* **101**, 233401-1–233401-4 (2008).
- ²⁷J. Tang, A. R. W. McKellar, X.-G. Wang, and T. Carrington, "Theoretical and experimental study of the infrared spectra of He₂-CO₂," *Can. J. Phys.* **87**, 417–423 (2009).
- ²⁸A. V. Potapov, L. A. Surin, V. A. Panfilov, B. S. Dumesh, T. F. Giesen, S. Schlemmer, P. L. Raston, and W. Jäger, "Rotational spectroscopy of the CO-para-H₂ molecular complex," *Astrophys. J.* **703**, 2108–2112 (2009).
- ²⁹S. Grebenev, B. G. Sartakov, J. P. Toennies, and A. F. Vilesov, "Spectroscopic investigation of OCS (p-H₂)_n (n = 1–16) complexes inside helium droplets: Evidence for superfluid behavior," *J. Chem. Phys.* **132**, 064501-1–064501-19 (2010).
- ³⁰P. L. Raston, Y. Xu, W. Jäger, A. V. Potapov, L. A. Surin, B. S. Dumesh, and S. Schlemmer, "Rotational study of carbon monoxide isotopologues in small ⁴He clusters," *Phys. Chem. Chem. Phys.* **12**, 8260–8267 (2010).
- ³¹P. L. Raston, W. Jäger, H. Li, R. Le Roy, and P.-N. Roy, "Persistent molecular superfluid response in doped para-Hydrogen clusters," *Phys. Rev. Lett.* **108**, 253402-1–253402-5 (2012).
- ³²P. L. Raston and W. Jäger, "Microwave spectroscopy of the seeded binary and ternary clusters CO-(pH₂)₂, CO-(pH₂)-He, CO-HD and CO-(oD₂)_{N=1,2}," *J. Chem. Phys.* **142**, 144308 (2015).
- ³³Z. Li, L. Wang, H. Ran, D. Xie, N. Blinov, and P. Roy, "Path integral Monte Carlo study of CO₂ solvation in ⁴He clusters," *J. Chem. Phys.* **128**, 224513-1–224513-7 (2008).
- ³⁴J. A. Ramilowski and D. Farrelly, "Fixed node diffusion Monte Carlo using a genetic algorithm: A study of the CO-⁴He_N complex, N = 1 . . . 10," *Phys. Chem. Chem. Phys.* **14**, 8123–8136 (2012).
- ³⁵A. Wairegi, A. Gamboa, A. D. Burbanks, E. A. Lee, and D. Farrelly, "Microscopic superfluidity in ⁴He clusters stirred by a rotating impurity molecule," *Phys. Rev. Lett.* **112**, 143401-1–143401-5 (2014).
- ³⁶K. K. Lehmann, "Rotations in liquid ⁴He: Lessons from a highly simplified model," *J. Chem. Phys.* **114**, 4643–4648 (2001).
- ³⁷M. Girardeau, "Relationship between systems of impenetrable Bosons and Fermions," *J. Math. Phys.* **6**, 516–523 (1960).
- ³⁸E. H. Lieb and W. Liniger, "Exact analysis of an interacting Bose gas. I. The general solution and the ground state," *Phys. Rev. A* **130**, 1605–1616 (1963).
- ³⁹A. Griffin, "New light on the intriguing history of superfluidity in liquid ⁴He," *J. Phys.: Condens. Matter* **21**, 164220-1–164220-9 (2009).
- ⁴⁰R. J. Donnelly, "The two-fluid theory of second sound in liquid helium," *Phys. Today* **62**(10), 34–39 (2009).
- ⁴¹J. Wilks and D. S. Betts, *An Introduction to Liquid Helium* (Clarendon Press, Oxford, U.K., 1987).
- ⁴²T. Giamarchi, *Quantum Physics in One Dimension* (Oxford University Press, 2003).
- ⁴³E. Haller, R. Hart, M. J. M. amd, J. G. Danzl, L. Reichsöllner, M. Gustavsson, M. Dalmonte, G. Pupillo, and H. Nägerl, "Pinning quantum phase transition for a luttinger liquid of strongly interacting bosons," *Nature* **466**, 597–600 (2010).
- ⁴⁴C. E. Chuaqui, R. J. LeRoy, and A. R. W. McKellar, "Infrared spectrum and potential energy surface of He-CO," *J. Chem. Phys.* **101**, 39–61 (1994).
- ⁴⁵R. A. Aziz, F. R. W. McCourt, and C. C. K. Wong, "A new determination of the ground state interatomic potential for helium dimer," *Mol. Phys.* **61**, 1487–1511 (1987).
- ⁴⁶J. K. Cullum and R. A. Willoughby, *Lanczos Algorithms for Large Symmetric Eigenvalue Computations*, Classics in Applied Mathematics Vol. 1 (SIAM, 2002).
- ⁴⁷G. H. Golub and C. F. van Loan, *Matrix Computations*, 3rd ed. (Johns Hopkins University Press, Baltimore, 1996).
- ⁴⁸Q. Ye, "Relative perturbation bounds for eigenvalues of symmetric positive definite diagonally dominant matrices," *SIAM J. Matrix Anal. Appl.* **31**, 11–17 (2009).
- ⁴⁹M. Dailey, F. M. Dopico, and Q. Ye, "Relative perturbation theory for diagonally dominant matrices," *SIAM J. Matrix Anal. Appl.* **35**, 1303–1328 (2014).
- ⁵⁰K. Sakmann, A. I. Streltsov, O. E. Alon, and L. S. Cederbaum, "Exact ground state of finite Bose-Einstein condensates on a ring," *Phys. Rev. A* **72**, 033613 (2005).
- ⁵¹E. H. Lieb, "Exact analysis of an interacting Bose gas. II. The excitation spectrum," *Phys. Rev.* **130**, 1616–1624 (1963).
- ⁵²H. Bethe, "Zur theorie der metalle. I. Eigenwerte und eigenfunktionen der linearen atomkette," *Z. Phys.* **71**, 205–226 (1931).
- ⁵³J. G. Muga and R. F. Snider, "Solvable three-boson model with attractive δ -function interaction," *Phys. Rev. A* **57**, 3317–3329 (1998).
- ⁵⁴K. Sakmann, <http://www.pci.uni-heidelberg.de/tc/usr/kaspar/ring.html>, 2011.
- ⁵⁵Wolfram Research, Mathematica, Wolfram Research, Inc., Champaign, IL, 2015.
- ⁵⁶O. E. Alon, A. I. Streltsov, K. Sakmann, and L. S. Cederbaum, "Continuous configuration-interaction for condensates in a ring," *Europhys. Lett.* **67**, 8–13 (2004).
- ⁵⁷B. G. Sartakov, J. P. Toennies, and A. F. Vilesov, "Infrared spectroscopy of carbonyl sulfide inside a pure ³He droplet," *J. Chem. Phys.* **136**, 134315-1–134316-8 (2012).
- ⁵⁸D. Mateo, M. Pi, J. Navarro, and J. P. Toennies, "A density functional study of the structure of small OCS@³He_N clusters," *J. Chem. Phys.* **138**, 044321-1–044321-8 (2013).
- ⁵⁹M. Geiner, O. Mandel, T. Esslinger, T. W. Hänsch, and I. Bloch, "Quantum phase transition from a superfluid to a Mott insulator in a gas of ultracold atoms," *Nature* **415**, 39–44 (2002).
- ⁶⁰R. Kanamoto, L. D. Carr, and M. Ueda, "Metastable quantum phase transitions in a periodic one-dimensional Bose gas. II. Many-body theory," *Phys. Rev. A* **81**, 023625-1–023625-13 (2010).
- ⁶¹D. Mateo, F. Gonzalez, and J. Eloranta, "Rotational superfluidity in small helium droplets," *J. Phys. Chem. A* **119**, 2262–2270 (2015).